



**HAL**  
open science

# Modeling the lava heat flux during severe effusive volcanic eruption an important impact on surface air quality

Jonathan Durand, Pierre Tulet, Maud Leriche, Soline Bielli, Nicolas Villeneuve, Andrea Di Muro, Jean-Baptiste Fillipi

## ► To cite this version:

Jonathan Durand, Pierre Tulet, Maud Leriche, Soline Bielli, Nicolas Villeneuve, et al.. Modeling the lava heat flux during severe effusive volcanic eruption an important impact on surface air quality. *Journal of Geophysical Research: Atmospheres*, 2014, pp.119. 10.1002/2014JD022034 . hal-01164000

**HAL Id: hal-01164000**

**<https://hal.science/hal-01164000>**

Submitted on 16 Jun 2015

**HAL** is a multi-disciplinary open access archive for the deposit and dissemination of scientific research documents, whether they are published or not. The documents may come from teaching and research institutions in France or abroad, or from public or private research centers.

L'archive ouverte pluridisciplinaire **HAL**, est destinée au dépôt et à la diffusion de documents scientifiques de niveau recherche, publiés ou non, émanant des établissements d'enseignement et de recherche français ou étrangers, des laboratoires publics ou privés.



Distributed under a Creative Commons Attribution 4.0 International License

# **1 Modeling the lava heat flux during severe effusive volcanic 2 eruption: an important impact on surface air quality**

Jonathan Durand,<sup>1</sup> Pierre Tulet,<sup>1</sup> Maud Leriche,<sup>2</sup> Soline Bielli,<sup>1</sup> Nicolas

Villeneuve,<sup>3</sup> Andrea Di Muro,<sup>3</sup> and Jean-Baptiste Fillipi<sup>4</sup>

---

<sup>1</sup>LACy, UMR 8105, CNRS - Université de

La Réunion, Météo-France

<sup>2</sup>LA, UMR 5560, CNRS - Université de

Toulouse III

<sup>3</sup>IPGP, UMR 7154, CNRS - Université Paris

Diderot

<sup>4</sup>SPE, UMR 6134, CNRS - Université de

Corse

3 **Abstract.** The Reunion Island experienced its biggest eruption of Piton de  
4 la Fournaise volcano during April 2007. Known as “the eruption of the century”,  
5 this event degassed more than 230 KT of SO<sub>2</sub>. These emissions led to impor-  
6 tant health issues, accompanied by environmental and infrastructure degrada-  
7 tions. This modeling study uses the mesoscale chemical model MesoNH-C to  
8 simulate the transport of gazeous SO<sub>2</sub> between April 2nd and 7th, with a focus  
9 on the influence of heat fluxes from lava. This study required the implementa-  
10 tion of a reduced chemical scheme, a basic surface model and an estimation of  
11 lava heat fluxes in the atmospheric model. The model was able to reproduce gen-  
12 eral trends of this eruption, in particular the crossing of trade wind inversion,  
13 the SO<sub>2</sub> surface concentration (with highest peak of SO<sub>2</sub> of 600  $\mu\text{g m}^{-3}$  observed  
14 April 4th for western Reunion locations), and the wet deposition associated to  
15 rainfall. A sensitivity study shows that without heat fluxes over the vent and the  
16 lava flow, simulated SO<sub>2</sub> surface concentration are up to 45 times higher than  
17 observed.

## 1. Introduction

### 1.1. Generalities

18 Volcanoes are one of the most important natural sources of air pollution, both during and be-  
19 tween eruptions [Oppenheimer, 2003]. It is essential for different areas of atmospheric science  
20 to have a good knowledge of volcanic volatile emissions in time and space, their atmospheric  
21 chemistry, physical and radiative effects. There are two different types of volcanoes: "reds"  
22 volcanoes characterized by relatively quiet effusive eruptions and transmitting any fluid lava  
23 in the form of castings, and "gray" volcanoes characterized by explosive eruptions and emit-  
24 ting pasty lava and ash in the form of pyroclastic flows. Each type of volcano is impacting  
25 the atmosphere in very different way, particularly in terms of injection depth and nature of the  
26 products ejected. Explosive volcanic eruptions such as those of El Chichon (Mexico) in 1982  
27 [Pollack *et al.*, 1983; Hoffman, 1987] and Mount Pinatubo in 1991 [McCornick *et al.*, 1995;  
28 Fiocco *et al.*, 1996; Robock, 2002], mainly affected climate because of radiative and chem-  
29 ical impact of the plumes formed by aerosols injected into the stratosphere [Solomon, 1999;  
30 Robock, 2000, 2002]. For effusive volcanic eruptions such as those of Piton de la Fournaise  
31 (Reunion Island, Indian Ocean), the problem is different. Knowledge of their atmospheric and  
32 environmental impacts in the troposphere and degassing processes has some shortcomings. By  
33 chemical oxidation reactions, volcanic gases such as SO<sub>2</sub>, which is predominant during the  
34 degassing of the lava, become acidic and can interact with the aerosol phase as precursors of  
35 particles through nucleation and/or condensation. These tropospheric volcanic aerosols play  
36 an important role in atmospheric radiation, directly by scattering and absorbing of short wave  
37 radiation, and indirectly by changing cloud cover and cloud properties [Hobbs *et al.*, 1982; Al-

38 *brecht*, 1989; *Kaufman et al.*, 2000; *Yuan et al.*, 2011a, b]. Tropospheric volcanic aerosols and  
39 gaseous compounds, especially sulfur dioxide, can also be source of risks to terrestrial ecosys-  
40 tems and health at local or regional scales [*Baxter et al.*, 1982; *Mannino et al.*, 1996; *Allen*  
41 *et al.*, 2000; *Delmelle et al.*, 2001]. Piton de la Fournaise is a typical basaltic shield volcano  
42 located on the Indian Ocean Island of Réunion and, as Etna and Kilauea, it is one of the world's  
43 most active effusive volcanoes, with an eruption occurring every 10 months in average [*Roult*  
44 *et al.*, 2012]. Reunion island is born 3 million years ago in the emergence of a gigantic vol-  
45 cano, in the southwest of the Indian Ocean at 21.06°S and 55.32°E. It presents on its 2512 km<sup>2</sup>  
46 a unique variety of landforms and landscapes with Piton des Neiges (3071m) being its highest  
47 point. The orographic influence on local dynamics of Reunion Island expected to be major. The  
48 interaction of the high mountainous terrain with the synoptic flow induces a large variability of  
49 wind field at local scale. The maritime and tropical location of the island, as well as the com-  
50 plexity of the terrain and wind exposure, imply a multitude of local circulations and weather,  
51 marked by large variations in temperature and precipitation. Modeling of local circulations is  
52 very complex to achieve in an environment like Réunion Island because it is the result of a  
53 complex interaction between topographic circulations, thermal breezes and local formation of  
54 clouds and precipitation. During an eruption, other parameters make modeling more difficult,  
55 including the effects of the dynamics of volcanic flows and thermal secondary effects associ-  
56 ated with lava flow. Few studies, as the Vog Measurement and Prediction Project (VMAP) on  
57 island of Hawaii (<http://mkwc.ifa.hawaii.edu/vmap/hysplit>), have been able to accurately rep-  
58 resent the distribution of volcanic pollution at characteristic scales of a volcanic island. The  
59 Piton de la Fournaise eruption of April 2007 presented all the characteristics of complex flow of  
60 sulfur dioxide with a temporal discontinuity between the highest concentrations of surface SO<sub>2</sub>

61 observed and the paroxysmal period of emission from the vent. The sulfur dioxide  $\text{SO}_2$  is the  
62 second gas emitted at the Piton de la Fournaise volcano after water  $\text{H}_2\text{O}$ , followed by carbon  
63 dioxide  $\text{CO}_2$  and hydrochloric acid  $\text{HCl}$ . The objectives in the framework of this case study  
64 are two-folds. First the paper aims to investigate the complex transport and distribution of the  
65 sulfur dioxide influenced by steep topography and three-dimensional atmospheric circulation.  
66 The second objective is to highlight the influence of the cloud scavenging and the heat fluxes  
67 on the  $\text{SO}_2$  surface concentration. For the latter, high resolution numerical simulations have  
68 been used to analyze the sensitivity of the heat fluxes on the volcanic pollutants. This paper  
69 starts with a brief description of April 2007 eruption as well as numerical methods (section 2).  
70 Section 3 is devoted to analyzing the estimation of the heat flux release during the eruption. The  
71 section emphasizes the influence of lava flow on the convection and its consequences on the  
72  $\text{SO}_2$  distribution.

## 1.2. Description of the April 2007 eruption of the Piton de la Fournaise

73 In April 2007, the Reunion's Island has known its biggest eruption of Piton de la Fournaise  
74 volcano at least three centuries [Michon *et al.*, 2013]. Within a month,  $210 \text{ Mm}^3$  of lava flowed  
75 out with  $90 \text{ Mm}^3$  reaching the sea. Above all, the collapse of the summit caldera caused signif-  
76 icant morphological change [Michon *et al.*, 2007]. Due to this nearby events and large environ-  
77 mental and civil protection impacts, this eruption is very well described in literature [Staudacher  
78 *et al.*, 2009; Vlastélic *et al.*, 2012; Barde-Cabusson *et al.*, 2011; Tulet and Villeneuve, 2010;  
79 Di Muro *et al.*, 2014]. After two short eruptive events (18 February and 30 March), a critical  
80 phase of the eruption started at 06 UTC on 2 April, located on the lower south-eastern part of the  
81 volcano ( $55^\circ 46' 25.5'' \text{ E}$  ;  $21^\circ 16' 54.6'' \text{ S}$  ,WGS84) at only 590m above the sea level and only  
82 3km from the coast (Figure 1). In less than eleven hours, two main lava streams reached the sea,

83 producing significant water vapor plumes with a very low pH due to strong presence of sulfuric  
84 and chlorohydric compound ( $\text{pH} < 2$ , *Staudacher et al.* [2009]). During the first two day, lava  
85 fountains up between 50m and 150m high were observed. From 4 April, MODIS sensor shows  
86 a significant increase of the lava flow rate until the 6th of April, where the peak of emissions of  
87 lava was observed (greater than  $200 \text{ m}^3/\text{s}$  at the vent, *Coppola et al.* [2009]; *Staudacher et al.*  
88 [2009]).  $\text{SO}_2$  emissions, proportional to lava emissions, were estimated at  $80 \text{ kg s}^{-1}$  the 4 April  
89 12 UTC,  $320 \text{ kg s}^{-1}$  the 5 April 12 UTC and  $1600 \text{ kg s}^{-1}$  the 6 April 12 UTC before a strong  
90 decrease until 8 April 12 UTC at  $55 \text{ kg s}^{-1}$ , and finally a constant emission of  $55\text{-}70 \text{ kg s}^{-1}$   
91 until 11 April [*Tulet and Villeneuve*, 2010]. The peak of degassing was simulated at  $1800 \text{ kg}$   
92  $\text{s}^{-1}$  on April 6, with the total budget estimated at 230kT, which is in agreement with the petro-  
93 logic estimation of 311kT [*Di Muro et al.*, 2014]. The Observatoire Volcanologique du Piton de  
94 la Fournaise (OVPF) recorded the 5 April at 20:48 UTC an earthquake of 4.8 magnitude syn-  
95 chronous with the caldeira collapse [*Michon et al.*, 2007; *Staudacher et al.*, 2009]. As described  
96 in *Tulet and Villeneuve* [2010] the location of this ash plume is well separate from the  $\text{SO}_2$  one,  
97 as well as the vapor plume. The 6 April, lava fountains reached more than 200m high, and there  
98 were several tens of individual lava flows from 2 to 20m wide [*Staudacher et al.*, 2009]. At this  
99 moment, the lava flow reaches its maximum lateral and longitudinal extents. In late 6 April,  
100 the intensity dramatically decreases, and the eruption became more “typical” compared to usual  
101 eruptions of Piton de la Fournaise. The 12th of April, the shallow seismicity came back at its  
102 highest, causing a new Dolomieu crater collapse. In the next days, the lava eruption intensity  
103 became steady with effusion measured at  $15\text{-}20 \text{ m}^3.\text{s}^{-1}$ . This last event continued until May 1st  
104 2007, the last eruption day.

### 1.3. ORA observations

105 ORA (Observatoire Réunionnais de l'air) provides daily monitoring of air pollution levels.  
106 It is equipped with several fixed and mobile stations along the Reunion coastline, measuring  
107 continuously primary and secondary pollutants. During the April 2007 eruption, 8 stations  
108 measured the SO<sub>2</sub> surface concentration from Saint Louis to Saint Denis passing through Cam-  
109 baie in the west (Figure 1). Data from these three stations are compared to simulations. The  
110 first day, surface concentration of SO<sub>2</sub> is very low with value under 20  $\mu\text{g m}^{-3}$  for all stations  
111 (Figure 2). The next day from 02 UTC, Saint Louis and Cambaie stations measured signifi-  
112 cant increases of SO<sub>2</sub> concentrations with a peak of more than 60  $\mu\text{g m}^{-3}$  for Cambaie and 200  
113  $\mu\text{g m}^{-3}$  for Saint Louis at 06 UTC. The 4th of April, new strong increases of surface concentra-  
114 tion have been measured by all stations located on the southwest and northwest coast. A peak  
115 of 600  $\mu\text{g m}^{-3}$  was observed at Cambaie and 587  $\mu\text{g m}^{-3}$  in Saint Louis at 13 UTC. A significant  
116 decrease followed this peak of SO<sub>2</sub> surface concentration, with SO<sub>2</sub> concentration falling below  
117 the 100  $\mu\text{g m}^{-3}$  threshold at the end of the day. The 5th, a slight increase appears at dawn (from  
118 03 UTC) with 200  $\mu\text{g m}^{-3}$  for Cambaie and 269  $\mu\text{g m}^{-3}$  for Saint Louis. Subsequently, from the  
119 5th (12 UTC) to the 10th of April (06 UTC), the concentration varied between 20  $\mu\text{g m}^{-3}$  to 120  
120  $\mu\text{g m}^{-3}$  for all west coast station except Saint Louis station, where brief peaks appeared for few  
121 hours on the 10th (345  $\mu\text{g m}^{-3}$ ) and the 24th (390  $\mu\text{g m}^{-3}$ ). The highest values measured by  
122 ORA are not in phases in time with the maximum emitted from the vent. This paradox needs a  
123 detailed study of sulfur dioxide transport.

## 2. Model description

### 2.1. Atmospheric model

124 The mesoscale non hydrostatic atmospheric model (MesoNH) developed by the Centre Na-  
125 tional de la Recherche Météorologique and the Laboratoire d'Aérodologie [*Lafore et al.*, 1998]  
126 has been used for the study. MesoNH can be used at all scales ranging from synoptic to large  
127 eddy scales (<http://mesonh.aero.obs-mip.fr/>). It can be run in a two way nested mode involving  
128 up to eight nesting stages. Different sets of parameterizations have been introduced for convec-  
129 tion [*Bechtold et al.*, 2001; *Pergaud et al.*, 2009], cloud microphysics [*Cohard and Pinty*, 2000],  
130 turbulence [*Bougeault and Lacarrere*, 1989], lightning [*Barthe et al.*, 2007], gaseous chemistry  
131 [*Suhre et al.*, 1998; *Tulet et al.*, 2003], cloud chemistry [*Leriche et al.*, 2000] and aerosols [*Tulet*  
132 *et al.*, 2005; *Grini et al.*, 2006].

### 2.2. Surface model

133 The SURFEx surface scheme is coupled with MesoNH to simulate surface processes, ther-  
134 modynamic and chemical exchanges with the atmosphere. (<http://www.cnrm.meteo.fr/surfex/>;  
135 *Masson et al.*, 2013.). SURFEx is composed by various parameterizations for natural land sur-  
136 face [*Noilhan and Mahfouf*, 1996; *Bougeault and Lacarrere*, 1989], urbanized area [*Masson*,  
137 2000], lakes and oceans [*Salgado and Le Moigne*, 2010] and chemistry and aerosols surface  
138 processes [*Tulet et al.*, 2003; *Mokhtari et al.*, 2012]. The coupling with the atmospheric model  
139 is performed by averaging the surface fluxes over a model grid box. Within SURFEx, the lava  
140 flow is represented by a line of potential heat flux emission, starting from the vent of the volcano  
141 at 21.28°S and 55.77°E to the coastline at 21.28°S and 55.80°E. This representation implies two  
142 major approximations for the lava flow. The first one is the misrepresentation of lava flow shape,  
143 as the observed lava flow has a triangular shape. The second is relative to the static represen-

144 tation of the lava under SURFEX, when the lava propagation is not integrated in time. The  
145 increasing surface of lava flow and its heat flux is modeled by multiplying the line of potential  
146 emission with a coefficient proportional to the increase of the lava flow surface.

### 2.3. Model configuration

147 The simulation starts at 00 UTC on April 2nd 2007, and ends at 00 UTC on April 7th 2007.  
148 The simulation has two nested domains with Kessler microphysics scheme and TKE turbu-  
149 lence scheme (prognostic turbulent kinetic energy, one and a half order closure). The largest  
150 domain with high model grid spacing (2km) is centered over the Reunion island. The do-  
151 main extends over 330km from north to south and 450km from east to west. The second  
152 domain covers only the Reunion Island and its coastline with a horizontal model grid spac-  
153 ing of 500m. The vertical grid is composed of 72 levels for both models stretching up to  
154 31km altitude with a first level 5m above ground level. Initial and lateral boundary condi-  
155 tions are extracted from ECMWF analysis for the meteorological fields and from MOCAGE  
156 (<http://www.cnrm.meteo.fr/gmgec/spip.php?article87>) for gaseous chemistry fields. The gas  
157 phase chemistry is resolved on both domains using the ReLACS chemical mechanism [*Crassier*  
158 *et al.*, 2009], which is a reduced version of RACM including the oxidation of sulfur dioxide by  
159 OH radical. In SURFEX, the entire SO<sub>2</sub> emission is released at the vent. This assumption is  
160 well correlated with the fact that the magma begin to degas when it reaches the vent and its sur-  
161 roundings. In consequence, with a 500m MesoNH horizontal model grid spacing, the location  
162 of SO<sub>2</sub> emission is well represented. A simulation protocol was implemented to limit the model  
163 drift by reinitializing the model dynamic (wind, humidity and temperature filed) in the middle  
164 of the simulation while the chemical fields have been preserved along the whole period (Figure  
165 3). A second simulation starts the 3rd at 18 UTC until the 4th of April at 00 UTC. This latter

166 provides at its end the dynamic fields refresh, while suppressing the need for model spin-up  
 167 (time taken by the model to reach equilibrium state). Finally, a new simulation starts the 4 April  
 168 at 00 UTC with the dynamic of simulation 2 and chemistry of simulation 1.

169 Sensitivity tests are made in this study to highlight the influence of heat fluxes in the transport  
 170 of volcanic pollutants and the influence of cloud chemistry in scavenging sulfur dioxide. The 3  
 171 simulations configurations are sum up in the table 1.

### 3. Estimations of thermodynamic emissions

#### 3.1. Heat flow estimation

172 Lava heat is released in the atmosphere from the core of an active flow by conduction through  
 173 the basal, lateral and surface crusts [*Oppenheimer, 1991; Klingelhofer et al., 1999; Quareni*  
 174 *et al., 2004*]. At the surface, heat losses are dominated by radiation ( $5 \times 10^4 \text{ W m}^{-2}$ ) and con-  
 175 vection ( $10^4 \text{ W m}^{-2}$ ), whereas conduction from the base to the ground is predominant ( $10^3 \text{ W}$   
 176  $\text{m}^{-2}$ , *Harris et al. [2005]*). For this study, only convective heat fluxes are implemented, with the  
 177 assumption that heat losses by conduction and by rain falling on the flow ( $250 \text{ W m}^{-2}$ , *Harris*  
 178 *et al. [2005]*) are negligible. As the influence of radiant heat fluxes is inversely proportional  
 179 to the square of the distance; we have also neglected it for our simulation. The heat flow by  
 180 convection is calculated from:

$$Q_{conv} = hc(T_{surf} - T_{air})$$

181 With  $hc$  the heat transfert coefficient estimated at  $50 \text{ W m}^{-2}$  by *Keszthelyi et al. [2003]*,  $T_{surf}$   
 182 the lava surface temperature and  $T_{air}$  the air temperature (290K). Estimation of the sensible heat  
 183 fluxes, and hence the lava cooling, is mainly controlled by the surface winds. The heat flux  
 184 relation to the wind from *Keszthelyi* observations are taken into account in our model (Figure

185 4). The surface covered by hot (1100°C) liquid lava flow and the crusted (400°C) lava is taken  
186 from the day by day observation given by *Bachèlery et al.* [2014] between April 2nd and 8th,  
187 allowing the estimation of the heat flow (in  $m^2$ ) from the ground.

#### 4. Sulfur transport during the April 2007 eruption of Piton de la Fournaise volcano using MesoNH atmospheric model

##### 4.1. SO<sub>2</sub> mass burden

188 Figure 5 represents the evolution of SO<sub>2</sub> mass burden simulated by MesoNH between April  
189 3rd and April 6th at 18 UTC. The first period until 4 April shows that the plume is oriented to  
190 the west with a maximum of mass burden of 210 DU. From April 5 and 6, the plume at the  
191 vent, above 5km ASL is oriented to the north with a large value (330 DU) over Reunion island.  
192 During this period, the strong presence of SO<sub>2</sub> in the north of Reunion Island indicates a plume  
193 separation. The change in direction between the two periods is due to the SO<sub>2</sub> plume crossing  
194 the inversion of trade winds around 3500m-4500m ASL. Below the inversion, a lower branch  
195 of the SO<sub>2</sub> plume is transported westward by the trade winds, while above, an upper plume is  
196 advected eastward. This analysis of SO<sub>2</sub> plume evolution in the first 4 days of the eruption is  
197 consistent with the study based on satellite data OMI and CALIOP by Tulet and Villeneuve  
198 (2010).

##### 4.2. Simulated SO<sub>2</sub> surface concentrations

199 In the morning of April 2, the SO<sub>2</sub> plume at the surface is oriented southwestwards, contourn-  
200 ing by the south the Piton de la Fournaise area. The plume is then transported along the coastline  
201 influenced by the trade winds circumventing the island, where a strong gradient of SO<sub>2</sub> appears.  
202 During this day, the SO<sub>2</sub> plume reaches Cambaie, at the northwest of the island with low surface  
203 concentration of SO<sub>2</sub> in order of some tens of  $\mu g m^{-3}$ . The strongest simulated concentrations

204 are located at low altitude, near Saint Joseph in the south, with  $350 \mu\text{g m}^{-3}$ . For other stations,  
205  $\text{SO}_2$  surface concentration is  $125 \mu\text{g m}^{-3}$  at Saint Louis in the southwest or a comparatively low  
206  $25 \mu\text{g m}^{-3}$  is observed in Sainte Thérèse in the northwest, while concentrations in Saint Denis  
207 to the north is even lower with  $1 \mu\text{g m}^{-3}$ . Not much changes occur the 3th of April, when the  
208 overall atmospheric dynamics confine the volcanic pollutants to the west of the island (Figure 6,  
209 dots represent ORA stations, Saint Denis at the north, Cambaie at the northwest and Saint-Louis  
210 at the southwest). Concentrations for the majority of the stations are stronger than the eve, with  
211  $200 \mu\text{g m}^{-3}$  at Saint Louis and  $75 \mu\text{g m}^{-3}$  at Cambaie and Sainte Thérèse (Figure 6). However,  
212 the strong  $\text{SO}_2$  gradient noted earlier is no longer present on April 3rd.  $\text{SO}_2$  distribution appears  
213 larger on the south and west side of La Reunion and to the west above the ocean.

214 Higher concentrations are simulated the 4th of April, with a peak of  $680 \mu\text{g m}^{-3}$  obtained at  
215 St. Joseph and  $350 \mu\text{g m}^{-3}$  obtained at St. Louis. For stations in the north of the island, the  
216 concentrations are close to of those April 3rd. The maximum  $\text{SO}_2$  concentration at the surface  
217 is thus located in the heights of the island, where high concentrations are simulated notably  
218 with more  $1000 \mu\text{g m}^{-3}$  in the heights above the city of Saint Joseph (south of Réunion Island).  
219 On the 5th of April, an increase of heat flow and a decrease in the stability of the atmospheric  
220 boundary layer allows the plume to reach higher altitude and in consequence be oriented directly  
221 to the northwest.

222 Finally, the 6 April, high concentrations are only simulated over the entire southern half of  
223 the island, with concentrations over  $5000 \mu\text{g m}^{-3}$ , 10 times the threshold recommended by  
224 European standards. Unfortunately, no observations are available in the south of the island to  
225 validate these very high-simulated concentrations the 6 April.

### 4.3. Comparison between MesoNH simulation and ORA data

From 2 to 5 April, the simulation succeeds to correctly reproduce general trends for all simulated stations on the island (Figure 7). On the 2nd, the SO<sub>2</sub> surface concentration given by MesoNH corresponds to ORA observations for these three stations with values below 15  $\mu\text{g m}^{-3}$  for Cambaie and Saint Denis and a peak of 200  $\mu\text{g m}^{-3}$  in the middle of the day for Saint Louis. On the 3rd, Saint Denis station did not record any presence of SO<sub>2</sub> while Cambaie station had a gradual increase with a peak of 85  $\mu\text{g m}^{-3}$  for ORA observation and 135  $\mu\text{g m}^{-3}$  in MesoNH simulation. Saint Louis has experienced a significant increase with a SO<sub>2</sub> surface concentration of 480  $\mu\text{g m}^{-3}$  measured by ORA and of 605  $\mu\text{g m}^{-3}$  simulated by MesoNH, once again in the middle of the day. The 4th of April, no changes occurred for Saint Denis, while a strong SO<sub>2</sub> increase appears at Cambaie with 500  $\mu\text{g m}^{-3}$  in MesoNH and 601  $\mu\text{g m}^{-3}$  for ORA observations. The same behaviour is also seen for Saint Louis station, with 585  $\mu\text{g m}^{-3}$  observed against a strong over concentration simulated value of 1135  $\mu\text{g m}^{-3}$ . It is important to note that this latter station is positioned on a very strong gradient of SO<sub>2</sub> (1135  $\mu\text{g m}^{-3}$  to 220  $\mu\text{g m}^{-3}$  at 5km away). This strong increase is immediately followed by a sharp decrease at the end of the day, with value below 150  $\mu\text{g m}^{-3}$  for Cambaie and 200  $\mu\text{g m}^{-3}$  for Saint Louis. On the 5th SO<sub>2</sub> concentration varies between 30 to 200  $\mu\text{g m}^{-3}$  for Cambaie, and 10 to 300  $\mu\text{g m}^{-3}$  for Saint Louis except in the evening (18 UTC) where the simulation does not succeed to keep low concentration values (550  $\mu\text{g m}^{-3}$  simulated instead of 35  $\mu\text{g m}^{-3}$  observed). For the simulation's last day, the SO<sub>2</sub> surface concentration given by the model is stronger than observations, with highest values of more than 450  $\mu\text{g m}^{-3}$  (against 45  $\mu\text{g m}^{-3}$  observed) at Cambaie and a peak of 590  $\mu\text{g m}^{-3}$  at Saint Louis instead of 55  $\mu\text{g m}^{-3}$ . The same anomaly appears for Saint Denis, when shortly after 00 UTC, the simulation gives a peak of 450  $\mu\text{g m}^{-3}$  instead of a total absence of

248 volcanic SO<sub>2</sub> highlighted by ORA measurements. Despite these orders of magnitude anomalies  
249 from the April 6th, and the global over exposition of SO<sub>2</sub> surface concentration for Saint Louis,  
250 SO<sub>2</sub> concentrations between 2 and April 7 are generally consistent with ORA measurements.  
251 The simulation succeed to recreate the paradoxical situation between the highest surface SO<sub>2</sub>  
252 concentration measured by ORA the 4 April whereas the paroxysmal intensity of the eruption  
253 is in the night (from 20 UTC) of the 5 April and on April 6th.

#### 4.4. Vertical transport above the eruption

254 The increased lava flow and its greater surface coverage between April 2 and 7 consequently  
255 involves an increase in heat flux over the lava flow. Heat flow for the first three days are moderate  
256 with an average of 12800 W m<sup>-2</sup>. Local circulation is still dominated by trade winds with  
257 surface winds around 5 m s<sup>-1</sup>. The plume reached 2.5km ASL. (under 100 μg m<sup>-3</sup>) and the  
258 highest SO<sub>2</sub> concentration value are close to the surface (23000 μg m<sup>-3</sup>). However, from April  
259 5th, the general trend is the increasing of trade winds (11 m s<sup>-1</sup> around the eruption zone). This  
260 increase induces more heat flux (22500 W m<sup>-2</sup> April 5) and a local breeze in the eruption area  
261 which creates a more efficient vertical transport of volcanic sulfur.

262 The surface warming and the heat flow associated with the lava flow generate atmospheric  
263 instability in the low layers of the troposphere. On Figure 8, the strong convection above the lava  
264 flow creates a large mixing area with a maximal negative vertical gradient of equivalent potential  
265 temperature of  $\partial\theta_e/\partial z = -1.5\text{K/km}$  between the lava and 7km ASL. Under the influence of the  
266 trade winds, the vertical structure of the plume in altitude is moving slightly westward. The  
267 vertical wind above the eruption reached 14 m s<sup>-1</sup> from 3 to 5km ASL. and transports SO<sub>2</sub> up  
268 to 8 km high (under 100 μg m<sup>-3</sup>), ie above the inversion zone trade winds situated between 2.5  
269 and 3.5 km of altitude. At this altitude the plume is in thermodynamic equilibrium with the

270 environment and oriented according to the wind direction, ie west/southwest. The plume is no  
271 longer transported to the west, but in the direction of Mauritius and Australia. High values of  
272 SO<sub>2</sub> concentration are modeled up to 6km (above 30000  $\mu\text{g m}^{-3}$ ) the 6 April (Figure 9, cross  
273 section in left panel corresponds to blue line (2 April) in Figure 1 and cross section in right  
274 panel corresponds to red line (6 April) ).

#### 4.5. Rainfall and aqueous chemistry

275 The 5 and the 6 April, strong clouds formations appears in the Piton de la Fournaise area. The  
276 associated accumulated rainfall simulated between 2 and 7 April 2007 by MesoNH is consistent  
277 with Meteo-France observations (Figure 10). Only the southeast weather station gives high  
278 rainfall value (67mm cumulated), whereas the western weather station recorded lower value  
279 (15mm and 6mm). One possible causes of concentrations overprediction for April 6th is that  
280 the scavenging of SO<sub>2</sub> by rain and cloud water leading to sulfuric acid formation is not taken  
281 into account in the simulation. However, Meteo-France measurements have shown that between  
282 April 2 and 7, the largest quantity of rain were observed only for the 6 April in the volcanic  
283 region. As MesoNH includes a cloud chemistry module [Leriche *et al.*, 2013] a sensitivity test  
284 was realized from April 5 18 UTC to April 7 00 UTC (limited period due to high computational  
285 cost) by activating this module. A simplified mechanism in aqueous phase was used including  
286 the oxidation of SO<sub>2</sub> into sulfuric acid by hydrogen peroxide, ozone and pernitric acid [Leriche  
287 *et al.*, 2003]. The module includes also the mass transfer kinetic for the exchange between  
288 the gas phase and liquid phases of soluble gases and their redistribution between cloud water  
289 and rainwater by microphysical processes (collision/coalescence leading to precipitation and  
290 sedimentation of raindrops leading to wet deposition).

291 One of the main consequence of cloud chemistry activation is a global decrease of SO<sub>2</sub> surface  
292 concentration due to SO<sub>2</sub> scavenging by rainfall and aqueous phase SO<sub>2</sub> chemistry transforma-  
293 tion inside clouds over Reunion Island. The 6 April at 13 UTC, the difference of SO<sub>2</sub> surface  
294 concentration between the simulation with cloud chemistry activated (AQ simulation) and ref-  
295 erence simulation (REF) reach up to  $-700 \mu\text{g m}^{-3}$  over the high terrain in the center of the island  
296 (Figure 11). The SO<sub>2</sub> surface concentration for the western coastline is  $200 \mu\text{g m}^{-3}$  lower for  
297 the AQ simulation than the REF simulation and for the Piton de la Fournaise area, a strong de-  
298 crease appears due to the proximity of the vent with the presence of high rainfall this day over  
299 the volcano. Generally, a 30% to 60% decrease is simulated by MesoNH, giving SO<sub>2</sub> surface  
300 concentrations close to ORA observations (Figure 12).

## 5. Influence of sensible heat fluxes in the transport of SO<sub>2</sub>

301 A sensitivity study was performed to characterize the influence of heat flux forcings over the  
302 vent and lava on the vertical transport of SO<sub>2</sub> (Figure 9). To do so, an additional simulation  
303 has been made without thermodynamic flux (NO-FLX) to highlight the contribution of these  
304 fluxes in the transport and the dispersion of sulfur dioxide. This simulation rapidly presents  
305 large discrepancy from the reference simulation (REF) as shown by Figure 13 in the differences  
306 of SO<sub>2</sub> concentration (in  $\mu\text{g m}^{-3}$ ) between the NO-FLX simulation and the REF simulation on  
307 the 3,4,5 and 6 of April at 13 UTC. A strong positive difference in concentrations appears for  
308 the whole southern part of the island with a maximum of  $32000 \mu\text{g m}^{-3}$ . The northwestern part  
309 of the island is also overexposed to higher concentrations of the order of  $500 \mu\text{g m}^{-3}$  for April  
310 3 and  $1000 \mu\text{g m}^{-3}$  from April 3 to 5. Conversely, negative anomalies are simulated the 4th  
311 of April for the northwest with less than  $340 \mu\text{g m}^{-3}$  compared to concentrations in the REF  
312 simulation. As a main consequence, concentrations obtained with the simulation NO-FLX are

313 also far from ORA measurements. In general, unrealistic peaks are simulated (Figure 14) with  
314 a factor of 5 to 35 in the south, and 5 to 10 in the northwest compared to ORA observations.  
315 Taking into account sensible heat flux from lava is therefore of prime importance as the NO-  
316 FLX simulation did not recreate correctly the spatial and temporal distribution of sulfur dioxide  
317 for the 2007 eruption of Piton de la Fournaise. Here, the lack of heat flux injection did not allow  
318 adequate vertical transport, essential to get an overall good representation of SO<sub>2</sub> distribution.  
319 As a general consequence we estimate that numerical modeling of the April 2007 eruption  
320 cannot be represented without heat flux correctly estimated and injected at the eruptive vent.

## 6. Conclusions

321 The objective of this study was to model fine scale spatial distribution of SO<sub>2</sub> degassed during  
322 the eruption of the Piton de la Fournaise in April 2007. It was necessary to adequately modeled  
323 the heat flux injection over the vent and lava flow to simulate the atmosphere dynamics that  
324 drives this SO<sub>2</sub> distribution. The simulation has been found to be in relatively good agreement  
325 with observations, and highlighted two phases. With moderate value of heat fluxes from lava  
326 flow ( $12800 \text{ W}\cdot\text{m}^{-2}$ ), the first phase, between April 2 and 4, shows a SO<sub>2</sub> plume still contained  
327 under the trade wind inversion at 3km ASL. The main consequence is a high SO<sub>2</sub> surface con-  
328 centration for western stations ( $600 \mu\text{g m}^{-3}$  for ORA observations,  $500 \mu\text{g m}^{-3}$  for simulation at  
329 Cambaie). The second phase, between April 5 and 7, corresponds to the eruption maximum in-  
330 tensity. This high intensity is accompanied by a strong increase in lava heat flux ( $22500 \text{ W m}^{-2}$ )  
331 that allows the SO<sub>2</sub> plume to cross the trade wind inversion, and reach an altitude of 8km ASL  
332 on the 6th of April. This deep convection reduces surface SO<sub>2</sub> concentration ( $600 \mu\text{g m}^{-3}$  to  $100$   
333  $\mu\text{g m}^{-3}$  in few hours at Cambaie), but the model fails to keep low SO<sub>2</sub> surface concentration on  
334 the last simulation day (peaks at  $400 \mu\text{g m}^{-3}$  instead of  $55 \mu\text{g m}^{-3}$  at the end of 6 April). These

335 over predictions were addressed by taking into account the cloud chemistry in a sensitivity study  
336 realized from 12 UTC on April 5 to April 7. During this period, the scavenging of SO<sub>2</sub> by rain  
337 water and cloud water significantly reduces SO<sub>2</sub> surface concentration, producing sulfuric acid  
338 and as a consequence acid rain. Overall, the reference simulation was largely in good agreement  
339 and within the same order of magnitude, with the observation values from ORA. To highlight  
340 heat flux influence, a second sensitivity study was performed, in which the heat fluxes from the  
341 vent and lava flow were totally suppressed. Without these additional contributions of heat flux,  
342 the simulated surface concentrations are up to 45 times higher than the observations. One of  
343 the main conclusions of the study is that heat flux above lava is a crucial parameter to take into  
344 account in order to reproduce correctly SO<sub>2</sub> distribution. This additional energy allows the de-  
345 velopment of strong convection that injects volcanic discharges over the atmospheric boundary  
346 layer. The heat flux model, although still imperfect by its surface representation, significantly  
347 improve the SO<sub>2</sub> spatial distribution, as shown in this study by respecting orders of magnitude  
348 compared to observations and by displaying correct temporal evolution of the simulated surface  
349 concentrations.

350 A perspective of improvement is the implementation of a new deep convection scheme to  
351 improve the representation of sub-grid convective transport in MesoNH model. The initial deep  
352 convection scheme from MESO-NH basic package is not adapted for an extreme event such  
353 as volcanic eruption. Indeed, some important processes are not taken into account or are not  
354 representative of a phenomenology of an eruption, such as the speed of ejection of gas and  
355 heat flow, or the absence of the mixing vertical processes. A strategy could be a coupling  
356 system between a more detailed lava surface model and MesoNH atmospheric model to better  
357 reproduce the distribution and evolution of the lava during the period.

358 **Acknowledgments.** We greatly acknowledge the MesoNH assistance, especially C.Lac and  
359 J.Escobar. Computer resources were provided by CINES (Centre Informatique National de  
360 l'Enseignement Supérieur <http://www.cines.fr/>, project no. lac6309) and CCUR (Centre de  
361 Calcul de l'Université de la Réunion) for the access to super-computer. We also thank ORA  
362 (<http://www.atmo-reunion.net/>) for free access to their data. Finally, we would like to thank  
363 OSU-R, OMNCG federation, Reunion University and LEFE/INSU program for funding this  
364 work.

## References

- 365 Albrecht, B. A. (1989), Aerosols, cloud microphysics, and fractional cloudiness., *Science*, 245.
- 366 Allen, A. G., P. J. Baxter, and C. J. Ottley (2000), Gas and particle emissions from soufrière  
367 hills volcano, montserrat, west indies: characterization and health hazard assessment., *Bull.*  
368 *Volcanol.*, 62.
- 369 Bachèlery, P., F. Saint-Ange, N. Villeneuve, B. Savoye, A. Normand, E. Le Drezen, A. Barrère,  
370 J. Quod, and C. Deplus (2014), Aâa lava flows into the sea, april 2007, piton de la fournaise  
371 volcano, la réunion island, *Active Volcanoes of the Southwest Indian Ocean: Piton de la Four-*  
372 *naise and Karthala. Active Volcanoes of the World. Springer-Verlag Berlin and Heidelberg.*
- 373 Barde-Cabusson, A., S. andÂ Finizola, A. Peltier, M. Chaput, N. Taquet, S. Dumont, Z. Duputel,  
374 A. Guy, L. Mathieu, S. Saumet, F. Sorbadère, and M. Vieille (2011), Structural control of  
375 collapse events inferred by self-potential mapping on the piton de la fournaise volcano (la  
376 reunion island), *J. Volcanol. Geotherm. Res.*, doi:doi: 10.1016/j.jvolgeores.
- 377 Barthe, C., J. Pinty, and C. Mari (2007), Lightning-produced nox in an explicit electrical scheme  
378 tested in a stratosphere-troposphere experiment: Radiation, aerosols, and ozone case study, *J.*

379 *Geophys. Res.*, *112*, doi:10.1029/2006JD007402.

380 Baxter, P. J., R. Stoiber, and S. N. Williams (1982), Volcanic gases and health: Masaya volcano,  
381 nicaragua, *Lancet*, *2*.

382 Bechtold, P., E. Bazile, F. Guichard, P. Mascart, and E. Richard (2001), A mass-flux convection  
383 scheme for regional and global models, *Quart. J. Roy. Meteorol. Soc.*, *127*, 869–886.

384 Bougeault, P., and P. Lacarrere (1989), Parametrization of orography induced turbulence in a  
385 meso-beta model, *Mon. Weather Rev.*, *117*.

386 Cohard, J., and J. Pinty (2000), A comprehensive two-moment warm microphysical bulk  
387 scheme, ii: 2d experiments with a non hydrostatic model, *Q. J. Roy. Meteorol. Soc.*, *126*.

388 Coppola, D., D. Piscopo, T. Staudacher, and C. Cigolini (2009), Lava discharge rate and effusive  
389 pattern at piton de la fournaise from modis data, *J. Volcanol. Geotherm. Res.*, *184*.

390 Crassier, V., K. Suhre, P. Tulet, and R. Rosset (2009), Development of a reduced chemical  
391 scheme for use in mesoscale meteorological models, *Atmos. Environ.*, *34*.

392 Delmelle, P., J. Stix, C.-A. Bourque, P. Baxter, J. Garcia-Alvarez, and J. Barquero (2001),  
393 Dry deposition and heavy acid loading in the vicinity of masaya volcano, a major sulfur and  
394 chlorine source in nicaragua, *Env. Sci. Tech.*, *35*.

395 Di Muro, A., N. Métrich, D. Vergani, M. Rosi, P. Armienti, T. Fougereux, E. Deloule,  
396 I. Arienzo, and L. Civetta (2014), The shallow plumbing system of piton de la fournaise vol-  
397 cano (la réunion island, indian ocean) revealed by the major 2007 caldera forming eruption,  
398 *Journal of Petrology*, *accepted in press*.

399 Fiocco, G., D. Fua, and G. Visconti (1996), The mount pinatubo eruption â effects on the atmo-  
400 sphere and climate, *Springer- Verlag*.

- 401 Grini, A., P. Tulet, and L. Gomes (2006), Dusty weather forecast using the mesonh atmospheric  
402 model, *Journal of Geophysical Research*, 111.
- 403 Harris, A., J. Bailey, S. Calvari, and J. Dehn (2005), Heat loss measured at a lava channel and its  
404 implication for down-channel cooling and rheology, *Geological Society of America, Special  
405 paper 396*.
- 406 Hobbs, P. V., J.-P. Tuell, H. D.-A., L.-F. Radke, and M.-K. Eltgroth (1982), Particles and gases in  
407 the emissions from the 1980-1981 volcanic eruptions of mt. st. helens, *Journal of Geophysical  
408 Research*, 87.
- 409 Hoffman, D.-J. (1987), Perturbations to the global atmosphere associated with the el chichon  
410 volcanic eruption of 1982, *Rev. Geophys.*, 25.
- 411 Kaufman, Y. J., D. Tanra, and O. Boucher (2000), A satellite view of aerosols in the climate  
412 system, *Nature*, 419(6903).
- 413 Keszthelyi, L., A. Harris, and J. Dehn (2003), Observations of the effect of wind on the cooling  
414 of active lava flows., *Journal of Geophysical Research*, SDE 4-1.
- 415 Klingelhofer, F., M. Hort, H.-J. Kumpel, and H.-U. Schemincke (1999), Constraints on the for-  
416 mation of submarine lava flows from numerical model calculations., *Journal of Volcanologi-  
417 cal and Geothermal Research*, 92.
- 418 Lafore, J., J. Stein, N. Asencio, P. Bougeault, V. Ducrocq, J. Duron, C. Fischer, P. Hereil, P. Mas-  
419 cart, V. M. J. Pinty, J. Redelsperger, E. Richard, and J. V.-G. de Arellano (1998), The meso-nh  
420 atmospheric simulation system. part i: adiabatic formulation and control simulations, *ang*, 16,  
421 90–109.
- 422 Leriche, M., D. Voisin, N. Chaumerliac, A. Monod, and B. Aumont (2000), A model for tropo-  
423 spheric multiphase chemistry: application to one cloudy event during the cime experiment,

424 *Atmos. Environ.*, *34*, 5015–5036.

425 Leriche, M., L. Deguillaume, and N. Chaumerliac (2003), Modeling study of strong acids for-  
426 mation and partitioning in a polluted cloud during wintertime, *Journal of Geophysical Re-*  
427 *search*, *108*, doi:10.1029/2002JD002950.

428 Leriche, M., J. Pinty, C. Mari, and D. Gazen (2013), A cloud chemistry module for the 3-d  
429 cloud-resolving mesoscale model meso-nh with application to idealized cases, *Geosci. Model*  
430 *Dev.*, *6*, 1275–1298.

431 Mannino, D., S. Ruben, F. Holschuh, T. Holschuh, M. Wilson, and T. Holschuh (1996), Emer-  
432 gency department visits and hospitalizations for respiratory disease on the island of hawaii,  
433 *Hawaii Med. J.*, *55*.

434 Masson, V. (2000), A physically-based scheme for the urban energy balance in atmospheric  
435 models, *blm*, *94*, 357–397.

436 McCornick, M.-P., L.-W. Thomason, and C.-R. Trepte (1995), Atmospheric effects of the mt  
437 pinatubo eruption, *Nature*, *373*.

438 Michon, L., T. Staudacher, V. Ferrazzini, P. Bachelery, and J. Marti (2007), April 2007 collapse  
439 of piton de la fournaise: a new example of caldera formation, *Geophys. Res. Lett.*, *31*, doi:  
440 10.1029/2007GL031248.

441 Michon, L., A. Di Muro, N. Villeneuve, C. Saint-Marc, P. Fadda, and F. Manta (2013),  
442 Explosive activity of the summit cone of piton de la fournaise volcano (la réunion  
443 island): a historical and geological review, *J. Volcanol. Geotherm. Res.*, *263*, doi:  
444 10.1016/J.jvolgeores.2013.06.012.

445 Mokhtari, M., L. Gomes, P. Tulet, and T. Rezoug (2012), Importance of the surface size distri-  
446 bution of erodible material: an improvement on the dust entrainment and deposition (dead)

- 447 model, *Geosci. Model Dev.*, 5, doi:10.5194/gmd-5-581.
- 448 Noilhan, J., and J. Mahfouf (1996), The isba land surface parameterization scheme., *Global and*  
449 *Plan. Change*, 13, 145–159.
- 450 Oppenheimer, C. (1991), Lava flow cooling estimated from landsat thematic mapper infrared  
451 data: the lonquimay eruption (chile, 1989)., *Journal of Geophysical Research*, 96.
- 452 Oppenheimer, C. (2003), Climatic, environmental and human consequences of the largest  
453 known historic eruption: Tambora volcano (indonesia) 1815, *Progress in Physical Geog-*  
454 *raphy*, 27.
- 455 Pergaud, J., V. Masson, S. Malardel, and F. Couvreux (2009), A parameterization of dry ther-  
456 mals and shallow cumuli for mesoscale numerical weather prediction, *Boundary-Layer Me-*  
457 *teorology*, 132.
- 458 Pollack, J.-B., O.-B. Toon, E.-F. Danielsen, H. D.-J., and J.-M. Rosen (1983), The el chichon  
459 volcanic cloud - an introduction, *Geophys. Res. lett.*, 10.
- 460 Quareni, F., A. Tallarico, and M. Dragoni (2004), Modeling of the steady state temperature field  
461 in lava flow levees., *Journal of Volcanological and Geothermal Research*, 132.
- 462 Robock, A. (2000), Volcanic eruptions and climate, *Rev. Geophys.*, 38.
- 463 Robock, A. (2002), Pinatubo eruption - the climatic aftermath., *Science*, 295.
- 464 Roullet, G., A. Peltier, B. Taisne, T. Staudacher, V. Ferrazzini, A. Di Muro, and O. team (2012), A  
465 new comprehensive classification of the piton de la fournaise activity spanning the 1985â2010  
466 period. search and analysis of short-term precursors from a broad-band seismological station,  
467 *JVGR*, doi:10.1016/j.jvolgeores.2012.06.012.
- 468 Salgado, R., and P. Le Moigne (2010), Coupling of the flake model to the surfex externalized  
469 surface model., *Boreal Env. Res.*, 15.

- 470 Solomon, S. (1999), Stratospheric ozone depletion: A review of concepts and history., *Rev.*  
471 *Geophys.*, 37.
- 472 Staudacher, T., V. Ferrazzini, A. Peltier, P. Kowalski, P. Boissier, and al (2009), The april 2007  
473 eruption and the dolomieu crater collapse, two major events at piton de la fournaise (la reunion  
474 island, indian ocean)., *Journal of Volcanology and Geothermal Research*.
- 475 Suhre, K., C. Mari, T. Bates, J. Johnson, R. Rosset, Q. Wang, A. Bandy, D. Blake, S. Businger,  
476 F. Eisels, B. Huebert, G. Kok, R. Mauldin, A. Prevot, R. Schillawski, D. Tanner, and D. Thorn-  
477 ton (1998), Physico-chemical modeling of the first aerosol characterization experiment (ace  
478 1) lagrangian b, 1. a moving column approach., *Journal of Geophysical Research*, 103.
- 479 Tulet, P., and N. Villeneuve (2010), Large scale modeling of the transport, the chemical trans-  
480 formation and the mass budget of the sulfur emitted during the eruption of april 2007 by the  
481 piton de la fournaise., *Atmos. Chem. Phys. Discuss.*, 10, doi:10.5194/acpd-10-21357-2010.
- 482 Tulet, P., V. Crassier, F. Solmon, D. Guedalia, and R. Rosset (2003), Description of the  
483 mesoscale nonhydrostatic chemistry model and application to a transboundary pollution  
484 episode between northern france and southern england., *Journal of Geophysical Research*,  
485 108, doi:10.1029/2000JD000301.
- 486 Tulet, P., V. Crassier, F. Cousin, K. Suhre, and R. Rosset (2005), Orilam, a three moment log-  
487 normal aerosol scheme for mesoscale atmospheric model, on-line coupling into the mesonh-c  
488 model and validation on the escompte campaign., *Journal of Geophysical Research*, 110,  
489 doi:10.1029/2004JD005716.
- 490 Vlastélic, I., G. Menard, M. Gannoun, J.-L. Piro, T. Staudacher, and V. Famin (2012), Magma  
491 degassing during the april 2007 collapse of piton de la fournaise: The record of semi-volatile  
492 trace elements, *Journal of Volcanology and Geothermal Research*, 256.

493 Yuan, T., L. Remer, and H. Yu (2011a), Microphysical, macrophysical, and radiative signatures  
494 of volcanic aerosols in trade wind cumulus observed by the a-train, *Atmos.Chem.Phys*, *11*,  
495 7119–7132, doi:0.5194/acp-11-7119-2011.

496 Yuan, T., L. Remer, K. Pickering, and H. Yu (2011b), Observational evidence of aerosol  
497 enhancement of lightning activity and convective invigoration, *Geophys.Res.Lett.*, *38*, doi:  
498 1029/2010/GL046052.

Simulation	Period	Lava heat flux	Cloud chemistry
REF	04/02 00 UTC - 04/07 00 UTC	Yes	No
NO-FLX	04/02 00 UTC - 04/07 00 UTC	No	No
AQ	04/05 18 UTC - 04/07 00 UTC	Yes	Yes

**Table 1.** The 3 simulations configurations. REF is the reference simulation, NO-FLX is the simulation without heat fluxes from lava flows and AQ is the simulation with cloud chemistry activated

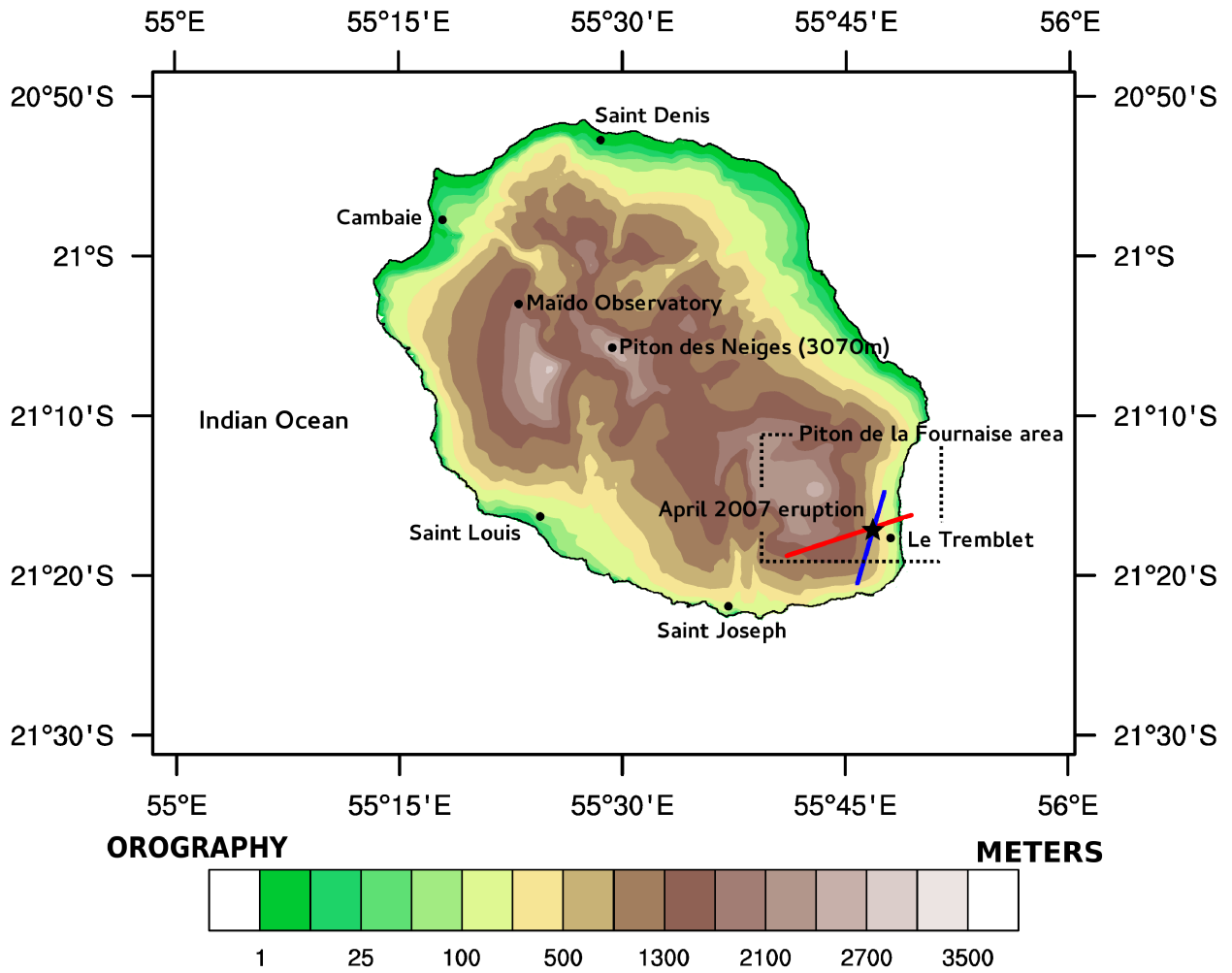


**Figure 1.** Orography and geographic situation of Reunion Island. The blue line and the red line in the Piton de la Fournaise area correspond respectively to the cross section of 2 April 2007 and 6 April 2007 describes in section 4-3.

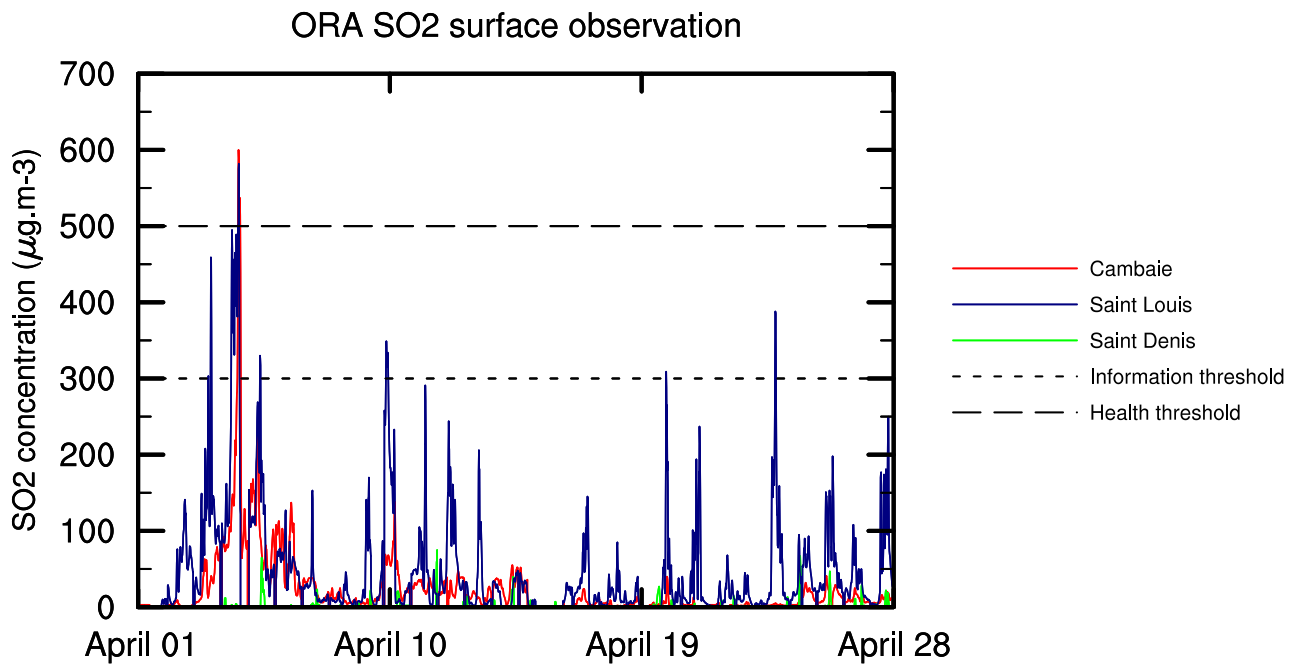


**Figure 2.** ORA measurements between April 1st and April 28th for Cambaie in the northwest (red), Saint Louis in the southwest (blue) and Saint Denis in the north (Green). Thin dashed line is the public information threshold and the large dashed line is the health threshold.

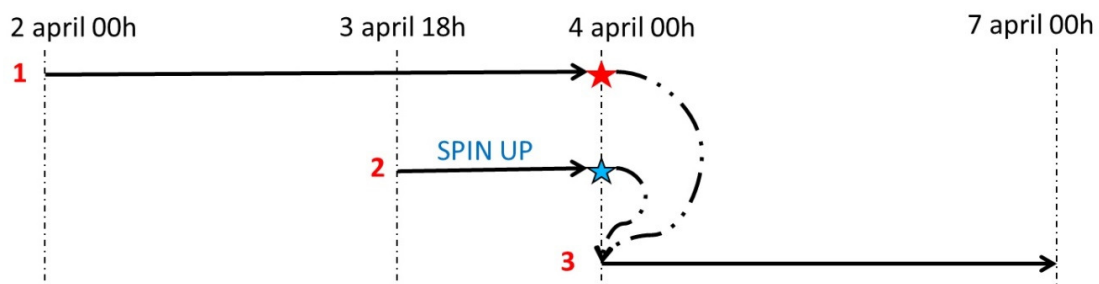


**Figure 3.** Updating the model dynamic: As a first step, the reference simulation begins the 2 April until 4 April 00 UTC (1). Then a new simulation begins April 3 18 UTC until 4 April 00 UTC (2). This latter will give the new model dynamics while avoiding the early simulation spin up. Finally, the REF simulation resumes the 4 April 00 UTC into the end, with chemical fields of (1) and model dynamic of (2).

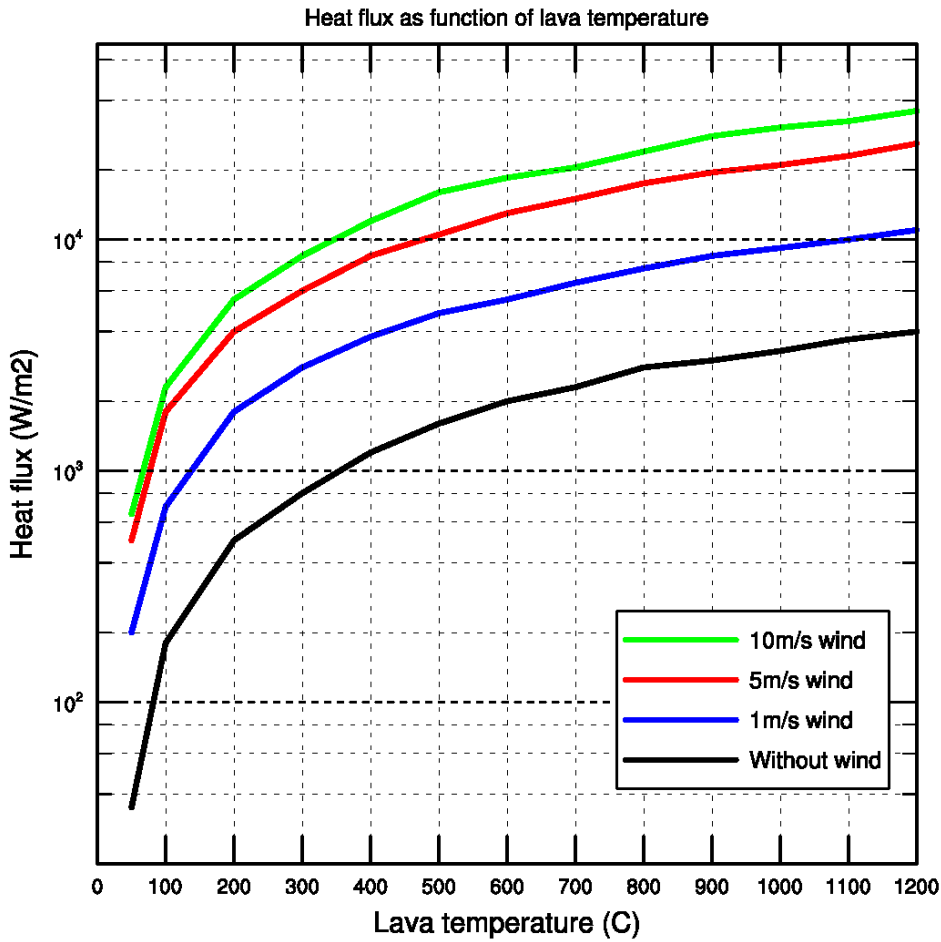


**Figure 4.** Heat flux evolution with lava surface temperature (Kezsthelyi et al, 2003). The green, red, blue and black lines represent heat fluxes respectively for 10 m s<sup>-1</sup>, 5 m s<sup>-1</sup>, 1 m s<sup>-1</sup> and without surface wind.

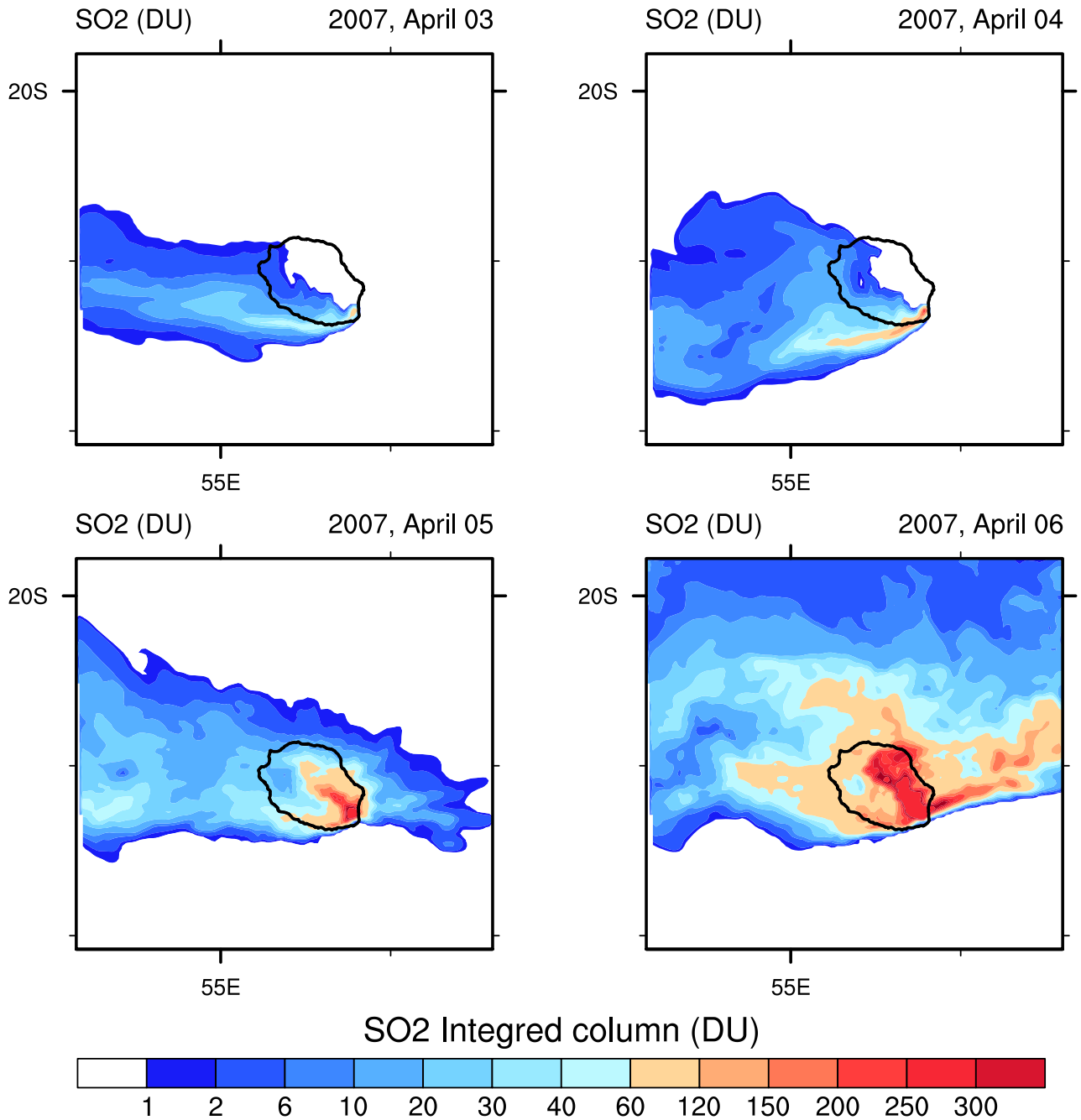


**Figure 5.** Integrated column of SO<sub>2</sub> (DU) between April 3 and April 6 at 13 UTC above the Reunion Island from first model domain (2km horizontal model grid spacing). April 2 and 3, the SO<sub>2</sub> plume, influenced by the trade winds below the thermic inversion, is oriented to the west. The 4 and 5 April, a large part of the SO<sub>2</sub> plume are crossing the trade winds inversion and is transported to the northeast.

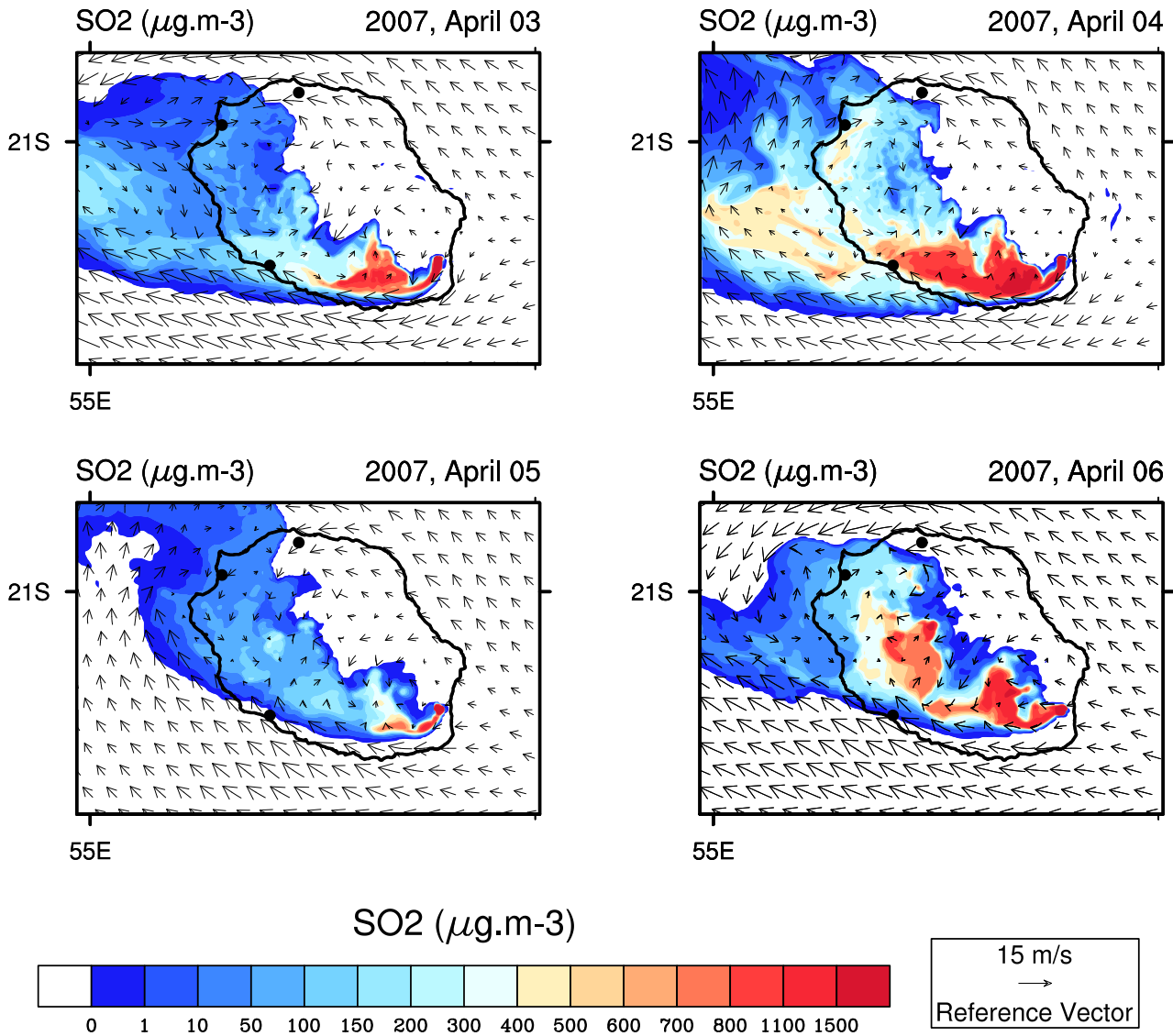


**Figure 6.** Surface concentration of SO<sub>2</sub> between April 3 and 6 at 13 UTC from MesoNH mesoscale atmospheric model smallest domain (500m horizontal model grid spacing)

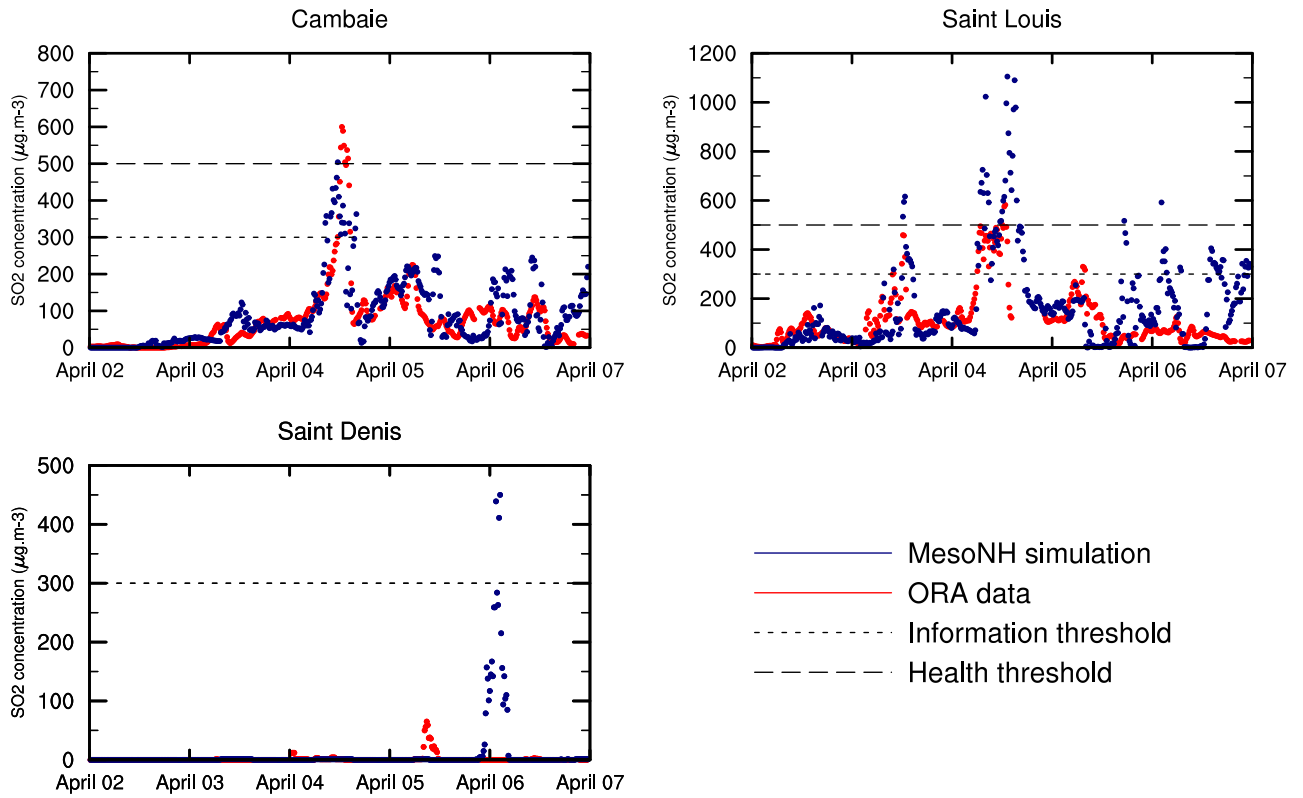


**Figure 7.** Comparison between ORA observation (blue points) and MesoNH simulation (red points) from April 2 to 7 April. The large dashed line is the health threshold while the thin dashed line is the information threshold.

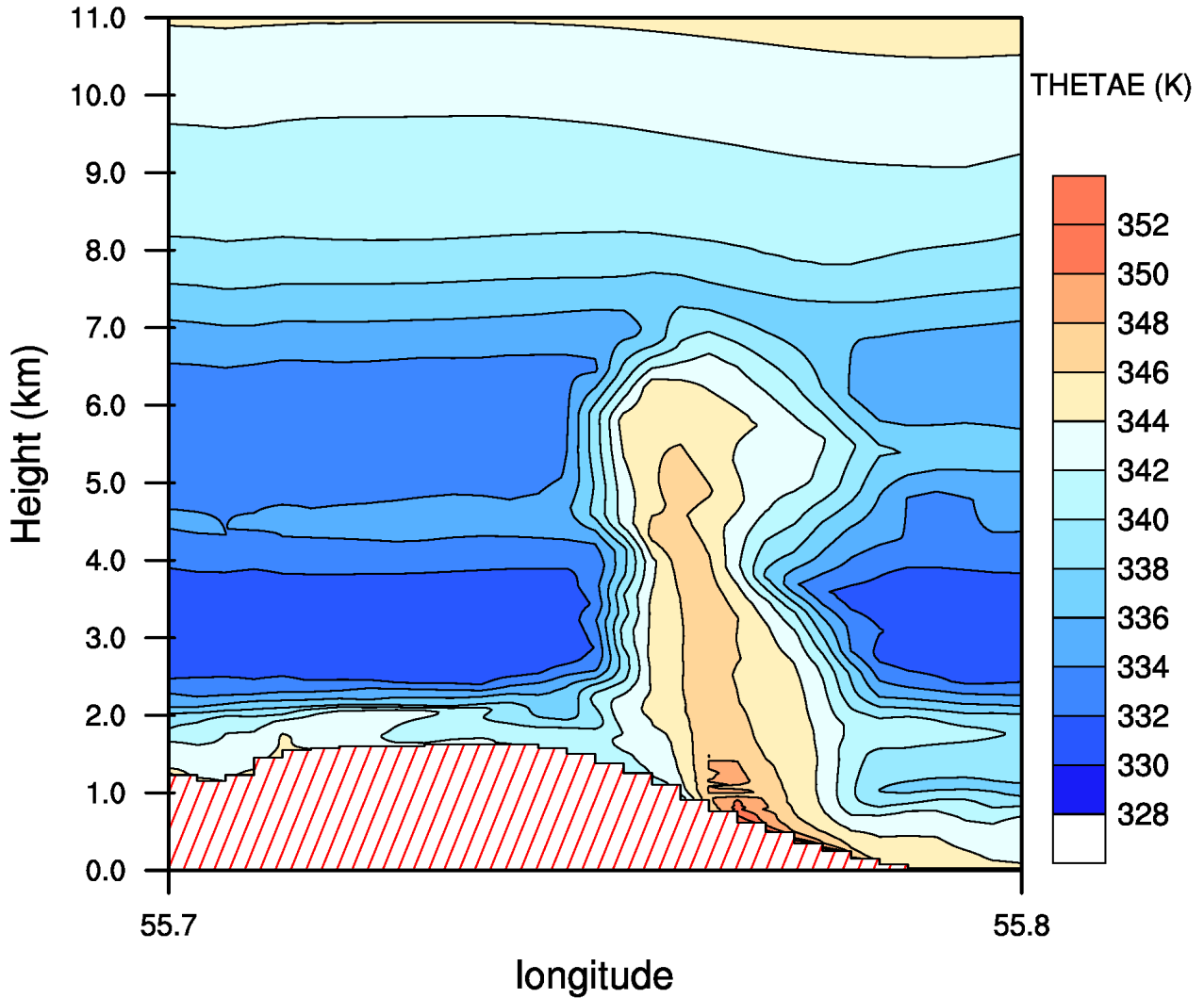


**Figure 8.** Cross section of equivalent potential temperature (K) for the 6th April at 13 UTC along red line in Figure 1. The strong convection above the lava flow creates a large mixing area with a maximal negative vertical gradient of equivalent potential temperature of  $\partial\theta_e/\partial z = -1.5\text{K/km}$  between the lava and 7km ASL. Under the influence of the trade winds, the vertical structure of the plume in altitude is moving slightly westward.

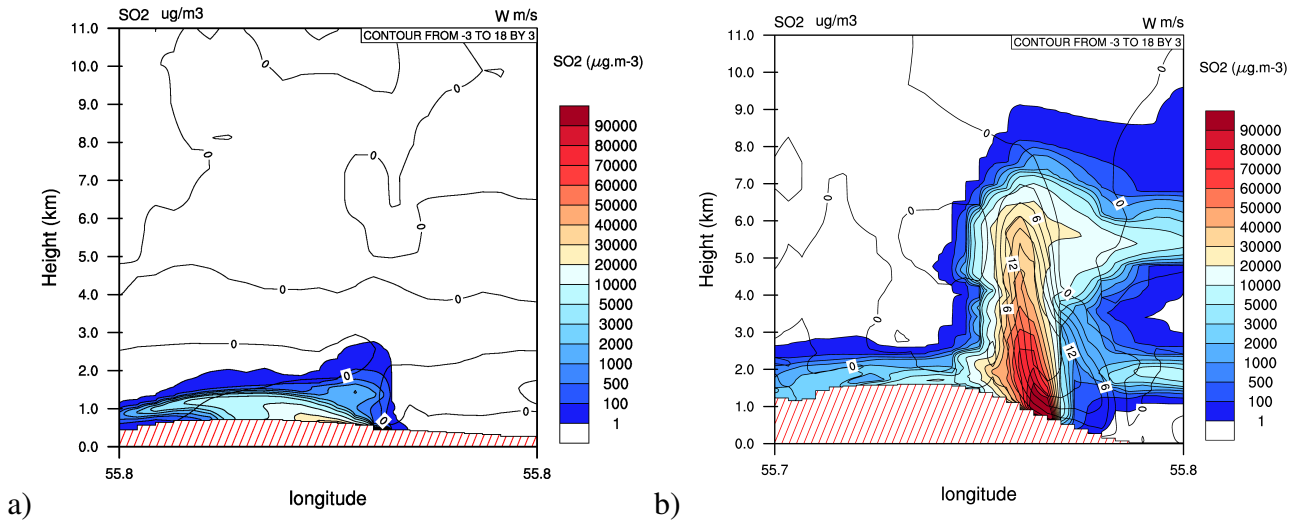
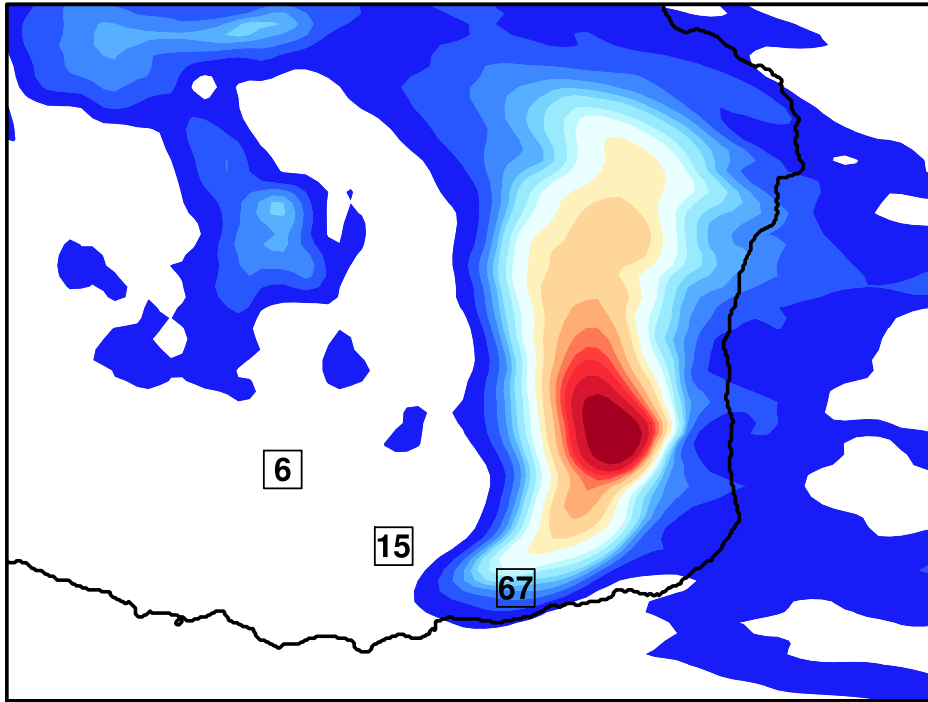


**Figure 9.** Cross section along SO<sub>2</sub> plumes for April 3 (left) and April 6 (right) at 13 UTC. The cross sections are not in the same direction due to change of plume orientation. The left panel corresponds to blue line in Figure 1, the right panel to red line. Color filling corresponds to SO<sub>2</sub> concentrations ( $\mu\text{g m}^{-3}$ ), isocontours values represent the upward velocity intensity ( $\text{m s}^{-1}$ ) generated by lava heat flow.

Accumulated rainfall (mm)

2007, April 07



Accumulated rainfall (mm)

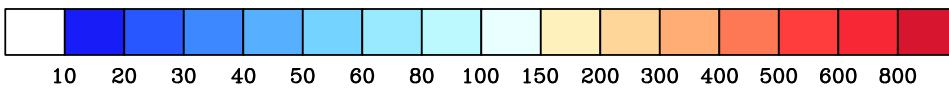


**Figure 10.** Accumulated rainfall given by MesoNH model between 2 and 7 April 2007. The numbers correspond to Meteo-France observations.

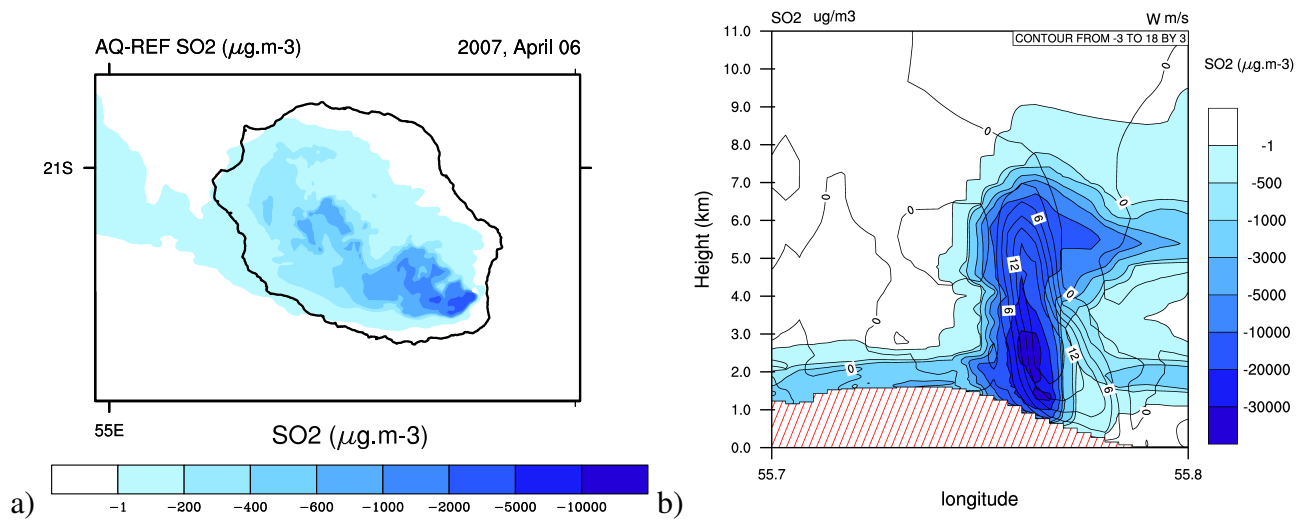


**Figure 11.** Difference of SO<sub>2</sub> concentration between AQ and REF simulation the 6 April at 13 UTC at the surface (left panel) and in the plume (right panel).

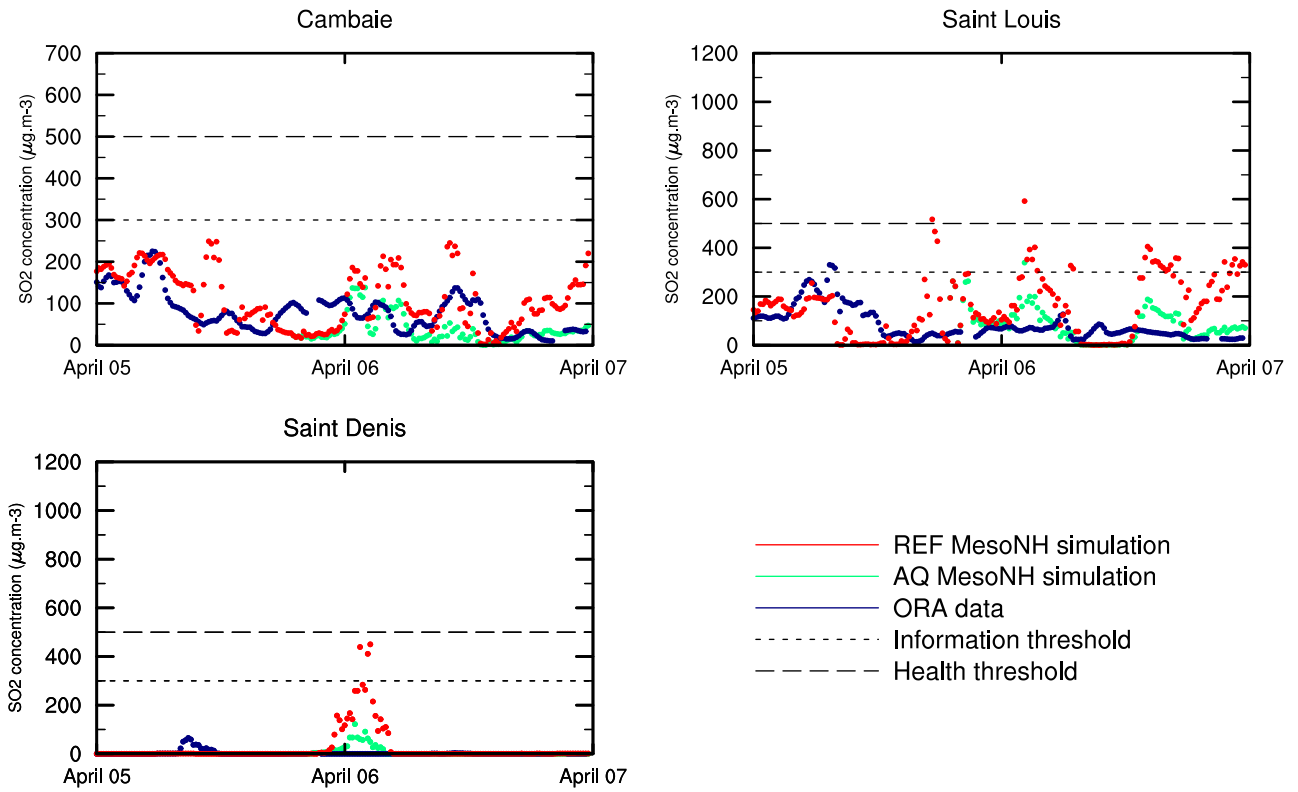


**Figure 12.** Comparison surface SO<sub>2</sub> concentration between between REF simulation and AQ simulation with observation providing by ORA.

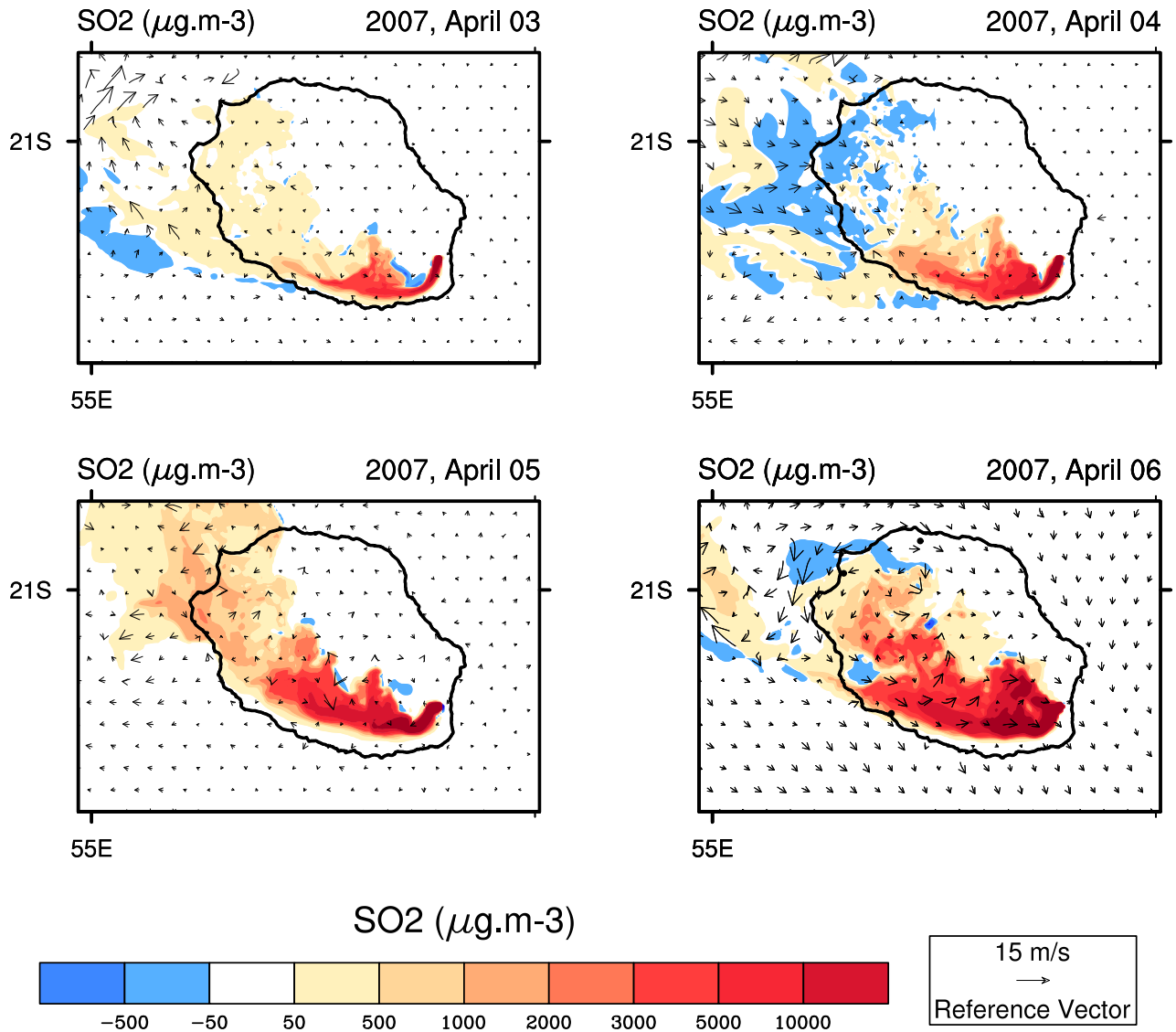


**Figure 13.** SO<sub>2</sub> concentration difference at the surface between NO-FLX and REF simulations, for April 3,4,5 and 6 2007 at 13 UTC. The arrows represent the difference of the wind field between NO-FLX simulation and REF simulation.

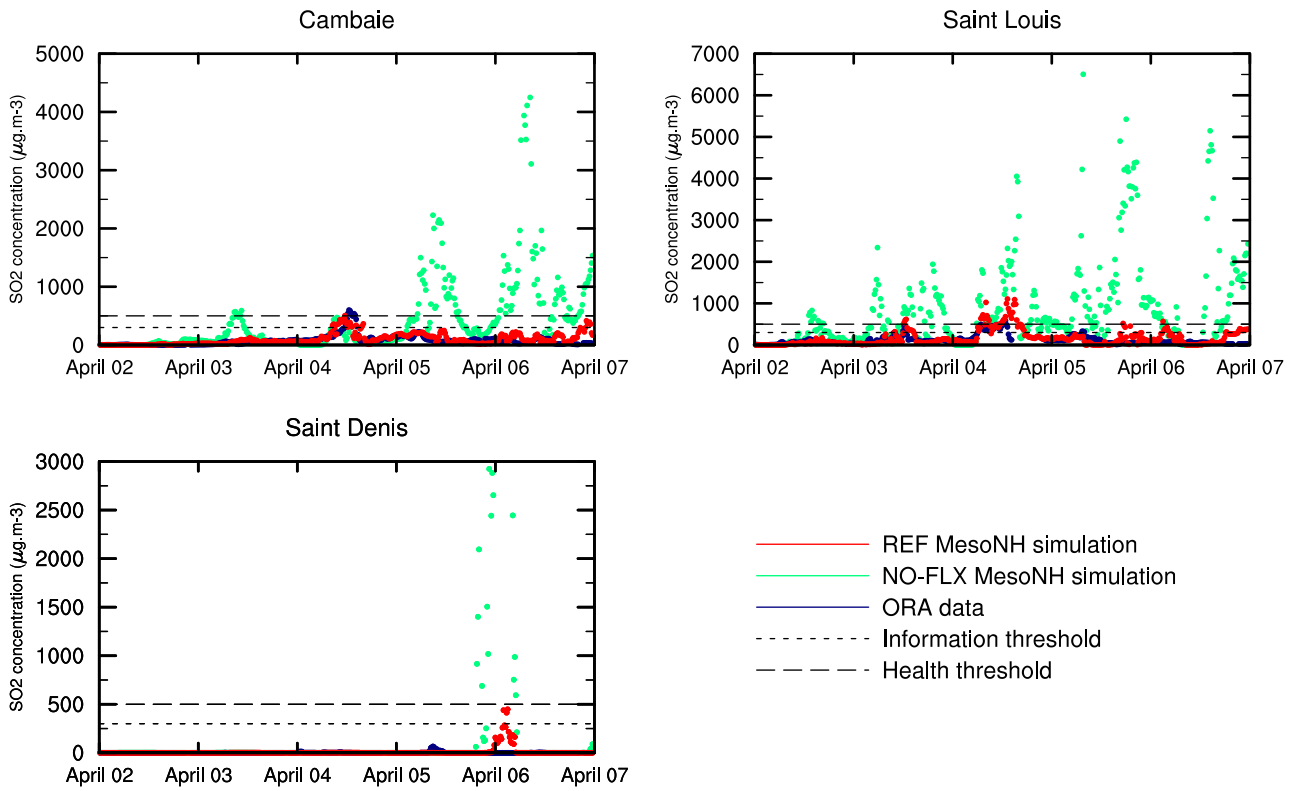


**Figure 14.** Comparison of surface  $\text{SO}_2$  concentration between NO-FLX simulation (green), REF simulation (red) and ORA measurements (blue). Thin dashed line is the public information threshold. Large dashed line is the health threshold.